ISSN 1330-3651 (Print), ISSN 1848-6339 (Online) https://doi.org/10.17559/TV-20210303201549
Original scientific paper

Mixing Enhancement of Mono-Disperse and Bi-Disperse Particles in a Cylindrical Drum Mixer Using Discrete Element Simulations

Seifeddine GARNEOUI, Péter KORZENSZKY*, Keppler ISTVÁN

Abstract: Numerous studies tackled the mixing behaviour of granular materials in a cylindrical drum mixer, however research regarding mixing enhancement by conceiving new designs of drum mixers is insufficient. Also, conducted studies to examine the mixing rate in various processes using the contact-based method rather than the variance-based method is unavailable. In this work, the discrete element method was used to study the mixing of mono-disperse and bi-disperse cohesionless solid particles in an inner-paddled rotating cylindrical drum mixer with different amounts of paddles and mixer rotational speeds. We found satisfactory mixing sates around the mixer periphery when compared with previously conducted real experiments to verify our DEM models. The contact-based method's so-called nearest neighbor was employed to quantitatively assess the different mixing scenarios. A better mixing rate is obtained when a cylindrical drum mixer has 8 uneven paddles installed along its horizontal axel and the mixer rotational speed is set at 48 rpm.

Keywords: discrete element method; drum mixer; granular material; homogeneity; mixing process

1 INTRODUCTION

Mixing of granular materials is of vital importance in many industries such as chemical, agricultural and pharmaceutical [1, 2]. The quality of the products mainly depends on the homogeneity criterion which is difficult to attain due to numerous physical and process parameters that may impact the product quality. In fact, an appropriate design of a mixer and proper parameters selection gives a better mixing efficiency, hence a better mixture quality.

Varying the rotational speed of a cylindrical drum mixer undoubtedly changes the motion of the loaded mass of particles. The material bed cascades inside the mixer causing a slipping to centrifuging profile motion [3]. The angle of repose is the inclination between the top surface of the rolled material bed and the horizontal surface that it is reposed on. Researchers revealed that the angle of repose increases by setting a higher drum speed [4], and the contrary when loading larger particles [5]. As the particles cascade, active zones also known as rapid flow layers and passive zones could be observed along the transverse section. Researchers have investigated those layers and came out with a yield line to separate them [6]. Many effects, including the avalanche effect identified by the rapid flow of the top layer of particles, could be observed during mixing based on the initial loading configuration and filling level [7]. Dead zones could take place due to inappropriate mixer design and setting of operating parameters [8]. For instance, Metcalfe et al., [7] observed that dead zones are caused by the static and dynamic angle frictions and other geometrical parameters.

Calculating the mixing rate is challenging in a drum mixer because different mixing mechanisms take place, such as convective and diffusive mixings in the radial and axial directions, respectively [9]. By knowing the mixing degree, the mixture quality can be identified, however sampling from various areas of the mixture is convoluted. Numerous experimental and numerical methods have been proposed to calculate the mixing index and estimate the mixture uniformity [10-12]. A simple technique is to collect samples by thrusting a probe thief in different areas of the mixture, however it impacts the state of particles located around the inserted probe thief [10]. Other image-based techniques have been utilized such as optical imaging [13] and near-infrared imaging [14], which are relatively expensive techniques. Researchers suggested a model to describe the mixture state based on some properties, namely: particle color, mass or density. Moakhter et al., [15] described the mixture state by dividing the mixture bed into vertical sections and tracking the axial coordinates of each vertical strip.

The mixing of granular materials in a drum mixer has been enhanced by an inclined axis of rotation [16], however using the novel structure of a drum mixer to improve the mixture and minimize dead zone formation is still scarce in literature. The Discrete Element Method (DEM) is a robust numerical technique used to investigate the flow of particles and assess the mixture state in any mixing process. For instance, Shen, Y. S. et al. [17], developed DEM models to see the effect of density on the mixing rate in a ribbon mixer and it showed that an extended mixing time is required when considering small particles. Zhijian Zuo et al. [18], revealed with DEM simulations, that decreasing the impeller offset would improve the mixing performance in an intensive mixer. This numerical method could be computationally expensive if a large number of small particles are considered. As an advantage, it treats the granular material bed as discrete elements. Each element is governed by the mechanical law of linear and rotational motions computed through time [19]. Guo and Curtis [20] have reviewed the application of the Discrete Element technique, mixing particles in a drum mixer with a fill fraction with a volume of more than 50% is challenging because dead zones tend to form less at a lower filling rates.

In this paper, we created a new structure for a cylindrical drum mixer and revealed its merit on the mixture of mono-disperse and bi-disperse solid spherical particles compared to a conventional cylindrical drum mixer using discrete element simulations. This paper is organized as follows; the first section presents the discrete element methodology, the second section describes the mixing rate used, reliability of the discrete element models is screened in section 4, results are interpreted in section 5, and our conclusions are drawn in the final section.

2 DISCRETE ELEMENT METHOD

The Discrete Element Method is a powerful numerical tool used to investigate the behavior of granular materials during processes such as packing, mixing, etc., by computing the Newtonian and contact force models in each iteration. It is capable of modelling either a small-scale or a large-scale system of solid elements. High-accuracy results could be achieved by the discrete element method when using a system composed of particles that have the same size, shape and physical parameters [21]. For instance, Lemieux et al., revealed that the DEM is reliable for modelling the flow of mono-disperse and bi-disperse particle systems in a V-blender [22].

The movement of every particle in DEM is described by the calculation of newton's equation of translation and rotation including the effect of gravity and contact forces. For a particle having a moment of inertia (I) and mass (m), the sum of forces acting on it describes the translational force and the sum of torques acting on it describes the rotational force. The effect of rolling friction was neglected in this work to simplify calculations. The Hooke's linear contact model implemented in LIGGGHTS code is used to calculate the normal and tangential forces between every two colliding particles [23]. The equations are written as follows:

$$m\frac{\mathrm{d}v_i}{\mathrm{d}t} = m_i g + \sum (F_{n,ij}^c + F_{t,ij}^c) \tag{1}$$

$\frac{\mathrm{d}v_i}{\mathrm{d}t}$ represents the acceleration of the translational motion, g is the acceleration of gravity, $F_{n,ij}^c$ and $F_{t,ij}^c$ are the normal force balance and the tangential force balance for two colliding particles i and j, and the general force balance equation for two colliding particles is given by:

$$F_{ij}^c = F_{n,ij}^c + F_{t,ij}^c = \left(F_{n,ij} - F_{n,ij}^d\right) + \left(F_{t,ij} - F_{t,ij}^d\right) \tag{2}$$

$F_{n,ij}^d$ and $F_{t,ij}^d$ are the normal and tangential damping forces, respectively. The sum of the normal contact force $F_{n,ij}$ and the tangential contact force $F_{t,ij}$ represents the contact force F_{ij} between particles i and j. They are calculated using LIGGGHTS code [23] as follows:

$$F_{n,ij} = \frac{16}{15} E_{ij} \sqrt{R_{ij}} \left(\frac{15 m_{ij} V_{cn,ij}}{16 \sqrt{R_{ij} E_{ij}}} \right)^{1/5} \delta_{n,ij} \tag{3}$$

$$F_{n,ij}^d = \sqrt{\frac{4 m_{ij} k_{n,ij}}{1 + \left(\frac{\pi}{\ln e}\right)^2}} V_{n,ij}^{\mathrm{rel}} \tag{4}$$

$$F_{t,ij} = \frac{16}{15} E_{ij} \sqrt{R_{ij}} \left(\frac{15 m_{ij} V_{ct,ij}}{16 \sqrt{R_{ij} E_{ij}}} \right)^{1/5} \delta_{t,ij} \tag{5}$$

$$F_{t,ij}^d = \frac{F_{n,ij}^d}{V_{n,ij}^{\mathrm{rel}}} V_{t,ij}^{\mathrm{rel}} \tag{6}$$

$\delta_{n,ij}$ and $\delta_{t,ij}$ are the normal and tangential overlaps between particles i and j, respectively; $V_{n,ij}$, $V_{t,ij}$ and V_{ij}^{rel} are the initial impact velocity in the normal direction, the initial impact velocity in the tangential direction and the relative velocity between two interacting particles i and j, respectively; $V_{n,ij}$ is the coefficient of static friction between particles i and j; E_{ij} is the equivalent Young's modulus; R_{ij} is the equivalent radius; m_{ij} is the equivalent mass and $k_{n,ij}$ is the normal stiffness. They are defined as follows:

$$\frac{1}{E_{ij}} = \frac{1-\nu_i^2}{E_i} + \frac{1-\nu_j^2}{E_j} \tag{7}$$

$$\frac{1}{R_{ij}} = \frac{1}{R_i} + \frac{1}{R_j} \tag{8}$$

$$\frac{1}{m_{ij}} = \frac{1}{m_i} + \frac{1}{m_j} \tag{9}$$

E_i, G_i, ν_i, R_i and m_i are the Young's modulus, shear modulus, Poisson's ratio, radius and mass of the particle i, respectively; E_j, G_j, ν_j, R_j and m_j are the Young's modulus, shear modulus, Poisson's ratio, radius and mass of the particle j, respectively.

The calculation cycle updates the position, velocity, and forces acting on every two particles at the end of every time-step. It begins with the detection of contact points and overlapping distances between particles, afterwards it calculates the contact forces through the force-displacement law, and subsequently the motion of particles is calculated through Newton's second law of motion. The setting of a time-step is of vital importance for convergence issue in any discrete element simulation. An explicit time integration scheme is implemented to solve the equations; therefore an adequate time-step should be considered. The Rayleigh time-step is frequently used to find the critical time-step which is the maximum value at which the simulation runs stably. It is calculated as follows:

$$\Delta T_{\mathrm{Rayleigh}} = \frac{\pi R}{1.63\upsilon + 0.8766} \sqrt{\frac{\rho}{G}}, \tag{10}$$

R, υ, ρ and G are the radius, Poisson's ratio, density, and shear modulus of particles, respectively. In our work, we have fixed the time-step in all simulations at 20% Rayleigh time.

3 HOMOGENEITY INDEX

Homogeneity index gives a quantitative understanding of the mixture of particles which could be obtained numerically by post-processing results from discrete element simulations. There are methods which are grid dependent, meaning that the mixing system should be divided into cells, then the index is calculated based on

statistical analysis by calculating the different number of particles of each type. The index is always in the interval [0, 1]. 0 indicates a total segregation state of mixture and 1 indicates a perfect state of mixture. Many conducted DEM studies have utilized the grid-dependent mixing index (so-called Lacey index) [24-26], this index is calculated as follows:

$$M = \frac{S^2 - S_0^2}{S_R^2 - S_0^2} \tag{11}$$

For an equally binary mixture of black and white particles; S^2 , S_0^2 and S_R^2 are the variance of black particle concentration in each cell, the variance of a fully unmixed material bed, and the variance of a fully mixed material bed, respectively. They are calculated as follows:

$$S^2 = \frac{1}{N-1}\sum_{i=1}^{n}(x_i - x_m)^2 \tag{12}$$

$$S_0^2 = x_m(1 - x_m) \tag{13}$$

$$S_R^2 = \frac{x_m(1 - x_m)}{n} \tag{14}$$

N is the number of cells. Knowing that the number of cells having no particles inside the system are neglected, n is the average number of particles per cell, x_i is the concentration of black particles in a cell i and x_m is the average concentration of black particles in the whole material bed.

This index lacks the ability to find the mixture state in a specific direction [27], moreover it showed an important level of uncertainty when different number of cells are used [28]. Fig. 1 shows the evolution we conducted of the Lacey index when mixing spherical solids in a cylindrical drum mixer. Evidently, Lacey mixing indices diverged when using different numbers of cells as described in Fig. 1. These uneven obtained results are due to the grid size applied to the DEM system for the calculations. Therefore, without a proper calibration, the Lacey index could be erroneous.

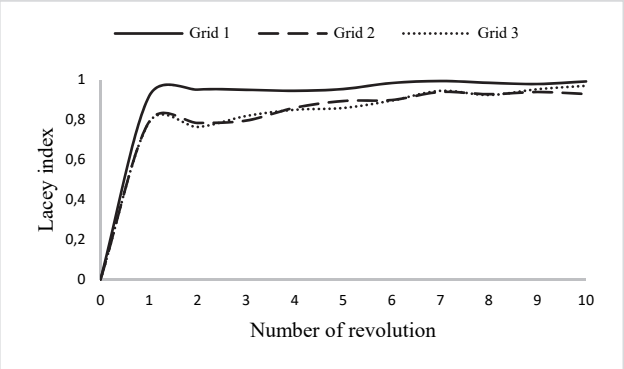

Figure 1 Evolution of the Lacey mixing indices according to grid systems utilized

On the other hand, grid-independent methods exist, which are non-sensitive to flow patterns. In this work, the nearest-neighbor method has been used. Rather than calculating the number of each particle's group in every cell, it finds a definite number of the nearest particles to every single particle by iteration, then it splits up the neighbors depending on their type. Fig. 3 presents an example showing how to calculate this grid-independent index in the case of a binary mixture with a 1:1 volume ratio of particles. In our work a large number of particles were used. For this purpose we wrote a java script to find the index in a short period of time by reading x, y and z coordinates of all the particles from a csv file. The following equation finds the nearest neighbor's mixing index for a whole material bed at a particular time.

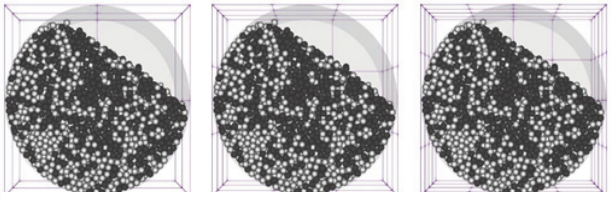

Figure 2 Different grid systems applied to the mixing domain for Lacey index calculations

$$M = \frac{1}{N_{\text{part}}}\sum_{N_{\text{part}}}\frac{2n_{\text{diff}}}{n_{\text{nb}}} \tag{15}$$

N_{part}, n_{diff} and n_{nb} are the total number of particles in the system, the number of different particles in terms of type and the number of neighboring particles, respectively

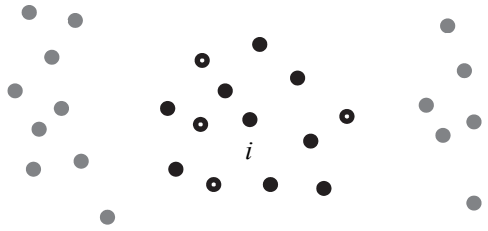

Figure 3 Illustrative case of the nearest-neighbor method

As illustrated in Fig. 3, the particle i has 8 identical particles among the 12 nearest particles, accordingly the index for the i^{th} particle is $2 \cdot 4/12 = 0.67$. The mixing index of the whole material bed is the average index of all particles.

In case of mixing different sizes of particles, for instance one group has n particles and another group has twice the number of particles of the first one, then the number of particles that should be considered as nearest to each particle should be scaled up by 1:2, meaning 24 particles are to be considered.

4 DISCRETE ELEMENT SIMULATION SYSTEM AND RELIABILITY ASSESSMENT

Cylindrical drum mixer assigned with acrylic material, having a diameter of 280 mm and a width of 140 mm, was created. The mixer was filled and maintained at 75%.

The mixer was filled at 70% for all the simulations with spherical glass beads. segregation state has been set before mixing by generating two groups of particles from separate inlets placed on the top of the mixer separated by

a cross-sectional splitter placed in the middle of the mixer in order to study the homogeneity of particles mixture from a totally inhomogeneous mixture state. The filling time of particles is 1 s. For the mono-disperse mixing case, the diameter of the two types of particles selected is 10 mm, and for the bi-disperse mixing case, the diameters of the two types of particles selected are 10 mm and 5 mm. A 1:1 filling volume ratio was maintained for all simulations inside the drum. After the particles have been inserted, the splitter was removed and the material bed settled down until it reached a stationary state in the mixer under the influence of gravity for 1 s time, followed by the rotation of the mixer vessel for 75 seconds, in order to ensure the maximum mixing rate. In this work, the micro-mechanical properties provided by Yanjie et al., [29] were used to define the mixer wall and particle materials and describe particle-particle and particle-wall interactions (Tab. 1).

Table 1 Micro-mechanical parameters used in simulations

Properties	Particle (glass spheres)	Mixer wall (acrylic sheet)	Particle-wall
Density, ρ / kg/m^3	2700	1800	-
Young's modulus, E / Pa	1e^7	1e^7	-
Coefficient of restitution, e	0.67	-	0.67
Poisson's ratio, υ	0.22	0.35	-
Coefficient of friction, μ	0.95	-	0.8

In this work used different configurations of the cylindrical drum by installing various numbers of paddles in the middle of the mixer. The length of paddles is uneven aiming to increase particle's randomization during the mixing process. We aimed to improve the mixing efficiency using these novel mixer designs, wherein a simple drum is also used in order to check the difference in terms of mixing efficiency. The mixer set-ups we used are detailed in Fig. 4.

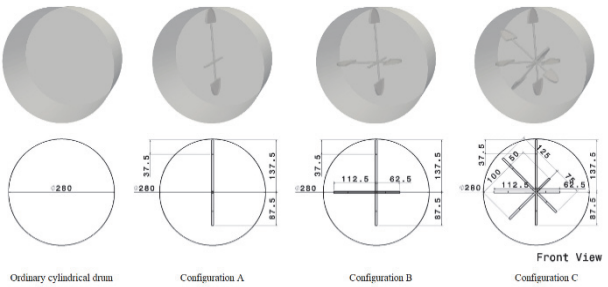

Figure 4 Set-ups of the cylindrical drum used in simulations

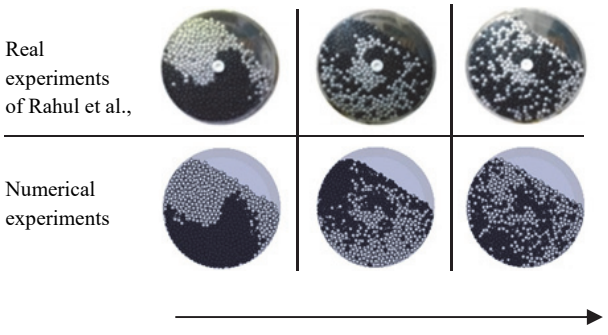

Figure 5 Mixing states of real experiments obtained from literature and numerical simulations at 4 rpm drum speed

Table 2 Design of numerical experiments

Simulation cases	Mixer set-up	Material bed	Mixer rotational speed
Case 1 to 4	Ordinary drum	Mono-disperse	8 rpm
	Configuration A		
	Configuration B		
	Configuration C		
Case 5 to 8	Ordinary drum	Bi-disperse	8 rpm
	Configuration A		
	Configuration B		
	Configuration C		
Case 9 to 15	Configuration C	Bi-disperse	16 rpm
			24 rpm
			32 rpm
			40 rpm
			48 rpm
			60 rpm
			80 rpm

The simulation cases are described in Tab. 2. Initially, simulation cases 1 to 4 and 5 to 8 were conducted at an 8 rpm fixed drum speed to check the efficacy of the different mixer designs in term of mixture uniformity for mono-disperse and bi-disperse materials, respectively. Eventually, the mixer speed was varied only for the finest mixer set-up in term of mixing efficacy for the bi-disperse material because it is more challenging, as shown in the results section. Simulation cases 9 to 15 tackled the impact of mixer rotational velocity (configuration C) on the bi-disperse mixture quality.

5 RESULTS AND DISCUSSIONS

LIGGGHTS-PUBLIC, version 3.8.0 (open-source software for simulating particles dynamics by the discrete element method, distributed by DCS Computing GmbH, Linz, Austria) was employed to perform all the runs, and PARAVIEW version 5.9.0 (open-source, multi-platform data analysis and visualization application) was used to visualize the results and generate simulations data. 4 groups of simulations were carried out, the first group involves 4 simulations to investigate the impact of the mechanisms described in Fig. 4 on the mixture quality of mono-sized particles. An identical number of simulations were also carried out to investigate the impact of the aforementioned mechanisms when mixing particles having different sizes. Then, 7 more simulations were conducted by varying the rotational speed of the best drum mechanism obtained to improve the mixing quality of bi-disperse particles and finding an optimal mixing model and speed for the drum. Finally, we furthered a sensitivity analysis of the mixture homogeneity on the coefficient of rotational friction by conducting numerical experiments at various values of the rotational friction coefficient. Results were post-processed by reading files generated from LIGGGHTS in PARAVIEW. The state of particles at a specific time could be visualized either near the mixer wall or in the middle of the mixer by clipping the system. Also, we could track particle velocity and their locations.

5.1 Mixing of Mono-Disperse Particles

Fig. 6 shows the variation in the mixing index with mixing times for the different drum set-ups. Reading the graphs reveals that "Configuration C" of the drum enhanced the mixture quality. This could be explained by

the approach that both particles near the mixer wall and paddles received maximum energies induced by them to improve the granular assembly, resulting in a diffusive mixing. Thus, paddles avoided dead zone formation in the middle of the mixer because without them in the mixer, little energy would be received among particles further from the mixer wall.

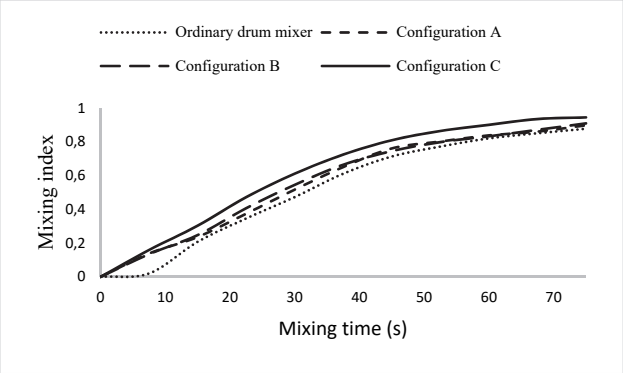

Figure 6 Variation in the overall mixing index of mono-disperse material bed during 75 s of mixing

5.2 Mixing of bi-disperse particles

In this part, we tackled the mixing of unequally sized particles. In this case, three mechanisms should be deemed: convection, diffusion, and segregation. The first two mechanisms sustain mixing. Convective mixing is also known as macro mixing which helps the granular material bed to turn around the mixer frame from one side to another and diffusive mixing involves the random displacement of a particle within a material bed, letting particles change their position relative to one another. However, segregation (the opposite term of mixing) disfavors mixing due to the so-called stratification phenomenon, as smaller particles tend to slip down the material bed through the voids between larger particles. This has been elucidated due to the uneven velocity speed of larger particles against smaller particles during mixing [30]. An appropriate mixing time should be selected to avoid insignificant over-mixing.

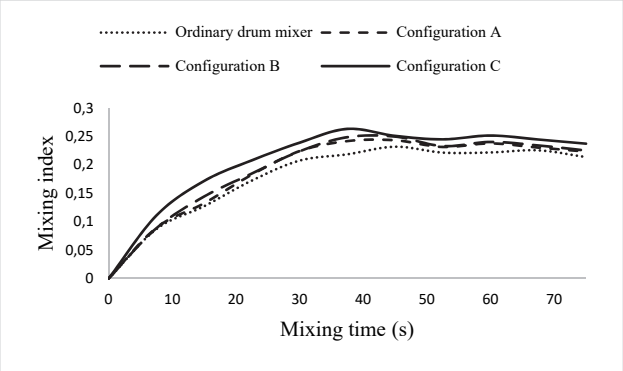

Figure 7 Variation in the overall mixing index of bi-disperse material bed during 75 s of mixing

Simulation cases 5 to 8 described in Tab. 2 were conducted. In the interest of improving the mixing state, various numbers of paddles, as described in section 5, were installed in the middle of the mixer along the axis to intensify particles mixing. Fig. 7 shows how the homogeneity index of the binary system progresses alongside mixing times for the different drum set-ups. Obviously, the paddled mixer improved the mixture. Also, a mixing-demixing transition is perceived from the curves of the mixing indices wherein the highest mixing degree is obtained at around 40 seconds of mixing time. Mixing beyond this time causes demixing.

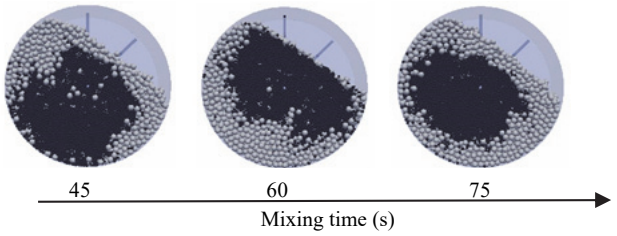

Figure 8 Variation in the overall mixing index of bi-disperse material bed during 75 s of mixing

Among advantages of the discrete element method, we can visualize particle distributions in the middle of the mixer. Observations of occupancy snapshots in the middle of the drum were described in Fig. 8. It can be seen from these snapshots that smaller particles tend to compact in the middle of the whole material bed, elucidating the low mixing degrees obtained even though paddles were being used in the drum.

5.3 Optimal Rotational Mixer Speed

According to results obtained in the previous sub-sections, it is obvious that the mixing of bi-disperse particles is rather complex and requires enhancement. For this purpose, we furthered simulations by gradually increasing the drum speed from 8 rpm to 16 rpm, 24 rpm, 32 rpm, 40 rpm, 48 rpm, 60 rpm and 80 rpm. Related homogeneity indices along the mixing process are illustrated in Fig. 9.

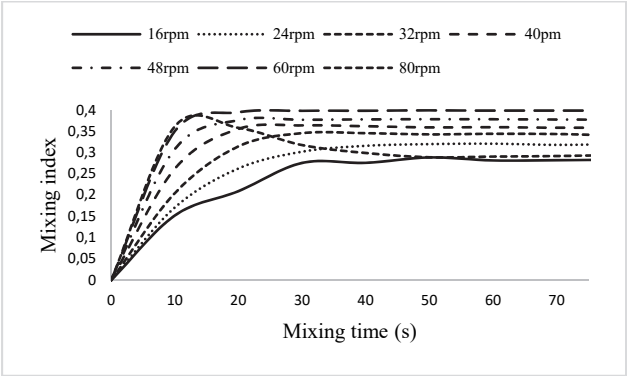

Figure 9 Variation in the overall mixing index of bi-disperse material bed during 75 s of mixing for various drum speeds

By increasing the drum speed, the mixture quality improves, whereas increasing the drum speed to above 60rpm is inefficacious as confirmed at 80 rpm.

5.4 Sensitivity Study of the Mixing Index on the Rolling Friction

As we neglected the coefficient of rotational friction to reduce calculation times, we furthered numerical

experiments to investigate the impact of the rolling friction on the mixture homogeneity in the drum mixer. According to previous studies about mixing of glass spheres in drums, the coefficient of rolling friction didn't exceed 0.01 between particles [2, 31]. As evidence, we introduced a range of values of the coefficient of the rotational friction between all particles, and between particles and the mixer wall from 0.001, 0.005, 0.01, and 0.025, after which the results were compared to the experiment that had no coefficient of rotational friction.

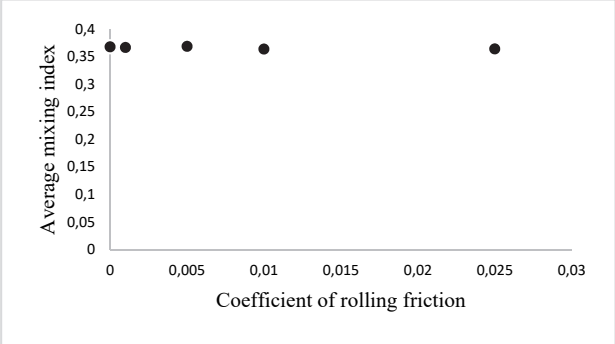

Figure 10 Variation of the average mixing index in relation to the coefficient of rolling friction (mixing of bi-disperse material case in "configuration C" set up of the mixer at 60 rpm drum speed)

Fig. 10 shows the results of the mixing indices for the different above-mentioned values of the coefficient of rotational friction. The mixing time was set at 25 seconds because previous results of the bi-disperse mixture with the "configuration C" mixer design showed that 60 rpm is the optimal speed of the drum and particle uniformity at this speed did not give rise to an increase after 25 s as it reached a steady state. Each value of the mixing index plotted in the graph is the average value of the indices calculated every 5 seconds of mixing time for every simulation. Results revealed that the coefficient of rotational friction has little to no effect on the mixture uniformity of particles in the cylindrical drum.

6 CONCLUSIONS AND RECOMMENDATIONS

The effects of paddle numbers and mixer rotational speeds have been investigated by using discrete element simulations. The number of paddles ranged between 2, 4 and 8 paddles, and the drum speed variations are 16, 24, 32, 40, 48, 60 and 80 rpm. The following conclusions could be drawn from the obtained results:

- Paddled drum mixer depicted by "configuration C" has the best mixing performance compared to other configurations. It has improved the mixture of the mono-disperse and bi-disperse mixtures by 15.36% and 13.28%, respectively compared to the non-paddled drum mixer.
- 60 rpm is the optimal drum rotational speed as it has improved the average mixing rate in 75 seconds of mixing time by 33.87%, 24.53%, 16.89%, 11.08% and 5.76% compared to 16 rpm, 24 rpm, 32 rpm, 40 rpm and 48 rpm, respectively. However, increasing the drum rotational speed adversely, impacted the mixing quality as setting the drum at 80 rpm worsened the mixture quality by 2.45% and 21.32% compared to 70 rpm and 80 rpm mixer speed, respectively.
- Sensitivity analysis showed that a maximum of 0.85% variance was obtained after setting a coefficient of rolling frictions ranging between 0 and 0.025, which demonstrates that the effect of the coefficient of rolling friction on the mixing rate in the drum is trivial.

As for recommendations, the effect of more complex shapes of particles on the mixing rate could be investigated.

Funding

This study was supported by the Stipendium Hungaricum Scholarship programme.

7 REFERENCES

[1] Huang, A.N. & Kuo, H.-P. (2014). Developments in the tools for the investigation of mixing in particulate systems - A review. *Advanced Powder Technology*, *25*, 163-173. https://doi.org/10.1016/J.APT.2013.10.007

[2] Marigo, M., Cairns, D. L., Davies, M., Ingram, A., & Stitt, E. H. (2012). A numerical comparison of mixing efficiencies of solids in a cylindrical vessel subject to a range of motions. *Powder Technology*, *217*, 540-547. https://doi.org/10.1016/j.powtec.2011.11.016

[3] Mellmann, J. (2001). The transverse motion of solids in rotating cylinders-forms of motion and transition behavior. *Powder Technology*, *118*(3), 251-270. https://doi.org/10.1016/S0032-5910(00)00402-2

[4] Yang, R. Y., Zou, R. P., & Yu, A. B. (2003). Microdynamic analysis of particle flow in a horizontal rotating drum. *Powder Technology*, *130*(1-3), 138-146. https://doi.org/10.1016/S0032-5910(02)00257-7

[5] Rao, S. J., Bhatia, S. K., & Khakhar, D. V. (1991). Axial transport of granular solids in rotating cylinders. Part 2: Experiments in a non-flow system. *Powder Technology*, *67*(2), 153-162. https://doi.org/10.1016/0032-5910(91)80152-9

[6] Boateng, A. A. & Barr, P. V. (1996). Modelling of particle mixing and segregation in the transverse plane in a rotary kiln. *Chemical Engineering Science*, *51*(17), 4167-4181. https://doi.org/10.1016/0009-2509(96)00250-3

[7] Metcalfe, G., Shinbrot, T., McCarthy, J. J., & Ottino, J. M. (1995). Avalanche mixing of granular solids. *Nature*, *374*, 39-41. https://doi.org/10.1038/374039a0

[8] McCarthy, J. J., Shinbrot, T., Metcalfe, G., Wolf, J. E., & Ottino, J. M. (1996). Mixing of granular materials in slowly rotated containers. *AIChE Journal*, *42*, 3351-3363. https://doi.org/10.1002/aic.690421207

[9] Sherritt, R. G., Chaouki, J., Mehrotra, A. K., & Behie, L. A. (2003). Axial dispersion in the three-dimensional mixing of particles in a rotating drum reactor. *Chemical Engineering Science*, *58*(2), 401-415. https://doi.org/10.1016/S0009-2509(02)00551-1

[10] Harwood, C. F. & Rippley, T. J. (1977). Errors associated with the thief probe for bulk powder sampling. *Powder Bulk Solution Technology*, *1*, 20-29.

[11] Realpe, A. & Velázquez, C. (2003). Image processing and analysis for determination of concentrations of powder mixtures. *Powder Technology*, *134*(3), 193-200. https://doi.org/10.1016/S0032-5910(03)00138-4

[12] Cleary, P. W., Metcalfe, G., & Liffman, K (1998). How well do discrete element granular fow models capture the essentials of mixing processes? *Applied Mathematical Modeling*, *22*(12), 995-1008. https://doi.org/10.1016/S0307-904X(98)10032-X

[13] Ehrhardt, N., Montagne, M., Berthiaux, H., Dalloz-Dubrujeaud, B., & Gatumela, C. (2005). Assessing the homogeneity of powder mixtures by on-line electrical

capacitance. *Chemical Engineering and Processing: Process Intensification*, *44*(2), 303-313. https://doi.org/10.1016/j.cep.2004.03.016
[14] Berntsson, O., Danielsson, L.-G., Johansson, M. O., & Folestad, S. (2000). Quantitative determination of content in binary powder mixtures using diffuse reflectance near infrared spectrometry and multivariate analysis. *Analitica Chemica Acta*, *419*(1), 45-54. https://doi.org/10.1016/S0003-2670(00)00975-2
[15] Moakher, M., Shinbrot, T., & Muzzio, F. J. (2000). Experimentally validated computations of flow, mixing and segregation of non-cohesive grains in 3D tumbling blenders. *Powder Technology*, *109*, 58-71.
[16] Widhate, P., Zhu, H., Zeng, Q., & Dong, K. (2020). Mixing of particles in a drum mixer with inclined axis of rotation. *Processes*, *8*(12). https://doi.org/10.3390/pr8121688
[17] Chandratilleke, G. R., Jin, X., & Shen, Y. S. (2021). DEM study of effects of particle size and density on mixing behaviour in a ribbon mixer. *Powder Technology*, *392*, 93-107. https://doi.org/10.1016/j.powtec.2021.06.058
[18] Zuo, Z., Gong, S., & Xie, G. (2021). Numerical investigation of granular mixing in an intensive mixer: effect of process and structural parameters on mixing performance and power consumption. *Chinese Journal of Chemical Engineering*, *32*, 241-252. https://doi.org/10.1016/j.cjche.2020.10.036
[19] Zhu, H. P., Zhou, Z. Y., Yang, R. Y., & Yu, R. B. (2007). Discrete particle simulation of particulate systems: theoretical developments. *Chemical Engineering Science*, *62*(13), 3378-3396. https://doi.org/10.1016/j.ces.2006.12.089
[20] Guo, Y. & Curtis, J. S. (2015). Discrete Element Method simulations for complex granular flows. *Annual Review of Fluid Mechanics*, *47*, 21-46. https://doi.org/10.1146/annurev-fluid-010814-014644
[21] Rajamani, R. K., Mishra, B. K., Venugopal, R., & Datta, A. (2000). Discrete element analysis of tumbling mills. *Powder Technology*, *109*(1-3), 105-112. https://doi.org/10.1016/S0032-5910(99)00230-2
[22] Lemieux, M., Bertrand, F., Chaouki, J., & Gosselin, P. (2007). Comparative study of the mixing of free-flowing particles in a V-blender and a bin-blender. *Chemical Engineering Science*, *62*(6), 1783-1802. https://doi.org/10.1016/j.ces.2006.12.012
[23] Gran model hooke model. DCS Computing GmbH, JKU Linz and Sandia Corporation. (2016).
[24] Lacey, P. M. C. (1954). Developments in the theory of particle mixing. *Journal of Applied Chemistry*, *4*, 257-268. https://doi.org/10.1002/jctb.5010040504
[25] Garneoui, S., Keppler, I., & Korzenszky, P. (2020). Mixing Enhancement of Wheat Granules in a Hopper Bottom Lab-Scale Mixer using Discrete Element Simulations. *FME Transactions*, *48*(4), 868-873. https://doi.org/10.5937/fme2004868G
[26] Ji, S., Wang, S., & Zhou, Z. (2020). Influence of particle shape on mixing rate in rotating drums based on super-quadric DEM simulations. *Advanced Powder Technology*, *31*(8), 3540-3550. https://doi.org/10.1016/j.apt.2020.06.040
[27] Godlieb, W., Gorter, S., Deen, N. G., & Kuipers, J. A. M. (2009). DEM and TFM simulations of solid mixing in a gaz-solid fluidized bed. *Seventh International Conference on CFD in the Minerals and Process Industries*.
[28] Bhalode, P. & Lerapetritou, M. (2020). A review of existing mixing indices in solid-based continuous blending operations. *Powder Technology*, *373*, 195-209. https://doi.org/10.1016/j.powtec.2020.06.043
[29] Li, Y., Xu, Y., & Jiang, S. (2009). DEM simulations and experiments of pebble flow with monosized spheres. *Powder Technology*, *193*(3), 312-318. https://doi.org/10.1016/j.powtec.2009.03.009
[30] Zhao, Y. & Cheng, Y. (2008). Numerical simulation of radial segregation patterns of binary granular systems in a rotating horizontal drum. *Acta Physica Sinica-Chinese Edition*, *57*(1), 322-328. https://doi.org/10.7498/aps.57.322
[31] Huang, A. N., Cheng, T. H., Hsu, W. Y., Huang, C. C., & Kuo, H. P. (2021). DEM study of particle segregation in a rotating drum with internal diameter variations. *Powder Technology*, 378(Part A), 430-440. https://doi.org/10.1016/j.powtec.2020.10.019

Contact information:

Seifeddine GARNEOUI, PhD Candidate
Hungarian University of Agriculture and Life Sciences, Gödöllő, Páter Károly u. 1, 2100, Hungary
E-mail: Seifeddine.g@gmail.com

Péter KORZENSZKY, Associate Professor
(Corresponding author)
Hungarian University of Agriculture and Life Sciences, Gödöllő, Páter Károly u. 1, 2100, Hungary
E-mail: korzenszky.peter.emod@szie.hu

Keppler ISTVÁN, Professor
Hungarian University of Agriculture and Life Sciences, Gödöllő, Páter Károly u. 1, 2100, Hungary
E-mail: keppler.istvan@gmail.com